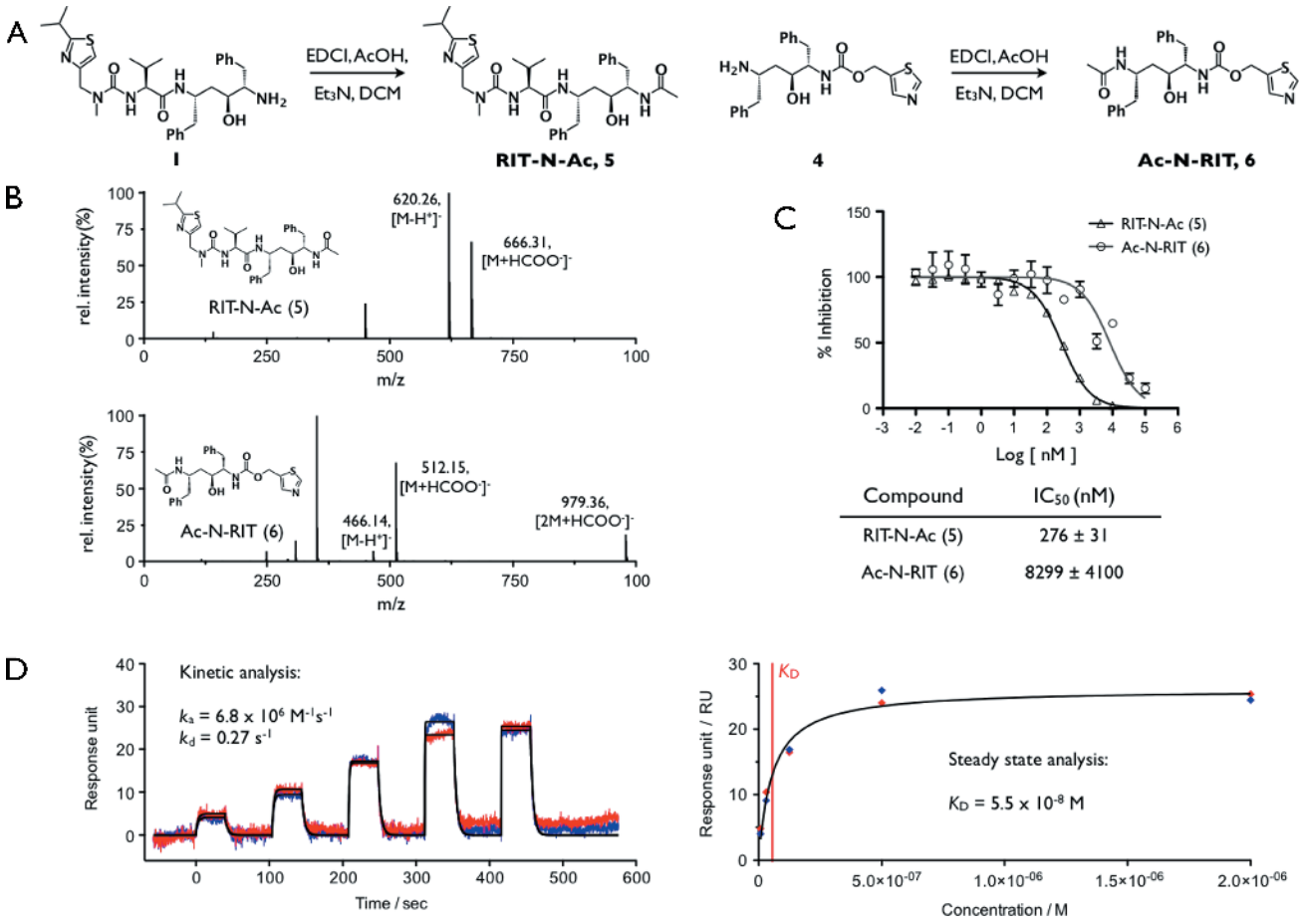

Figure W1. Synthesis and characterization of RIT-NH-Ac (**5**) and Ac-NH-RIT (**6**). (A) Synthetic schemes of **5** and **6**. (B) LC-MS analyses of purified of **5** and **6**. (C) Binding affinity data for **5** and **6** against human CTSE. (D) SPR binding data for the interaction of **5** with immobilized CTSE. Red and blue curves depict experimental data (two separate runs); best-fit models overlaid in black.

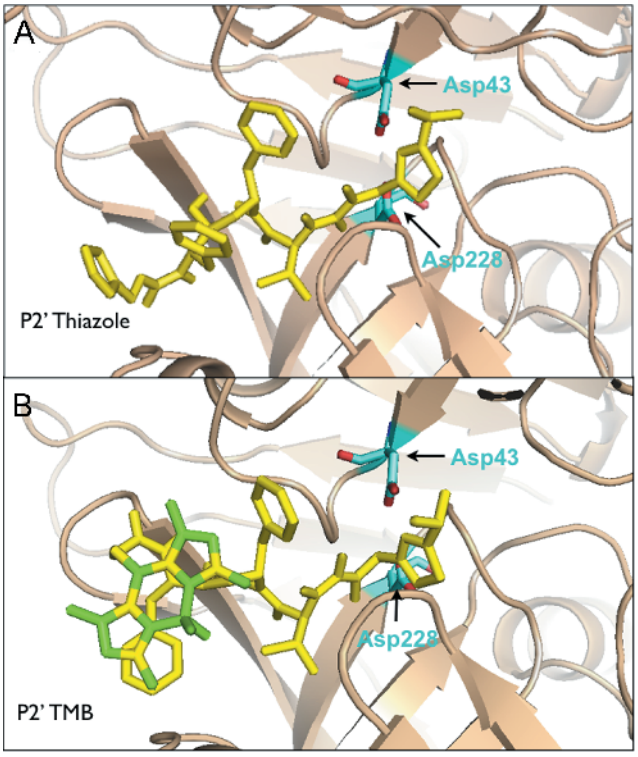

Figure W2. Modeling. Simulated docking of RIT (A) and RIT-TMB (B) with homology model of CTSE.

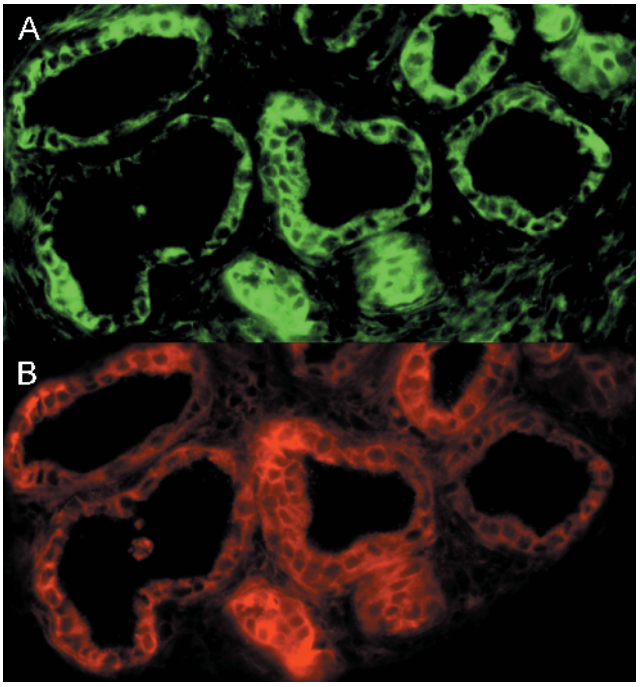

Figure W3. Immunofluorescent anti–CTSE/RIT-TMB double staining of tumor section excised from 10-week-old KRAS p53−/− model. (A) RIT-TMB (20 μM RIT-TMB for 1 hour). (B) Anti-CTSE immunofluorescence.

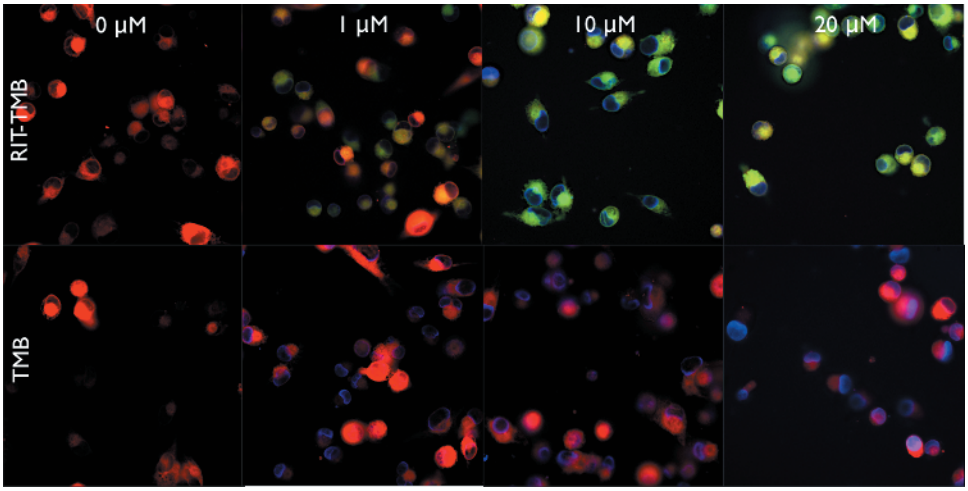

Figure W4. PaCa-2 CTSE-mCherry cells incubated with RIT-TMB and TMB (fluorochrome only). CTSE-mCherry (red), RIT-TMB and TMB (green), and 4′,6-diamidino-2-phenylindole (blue).

	Species	Comment	Western	mRNA
AsPC1	Human		ND	11.9
PANC1			0.3	2.9
PACA2			0.5	1
PACA2-CathE-mCherry		Transduced from PACA2	6.4	354396
PANC02	Mouse		0.5	ND
AH367		$Kras^{+/+}Ink4a/Arf^{-/-}$	0.5	ND

Figure W5. Relative quantification of CTSE protein and mRNA expression in PDAC cell lines.